Note: In this revised version, the symbol α used as the coefficient of the potential V(S) or in dynamic equations has been renamed α_V to avoid confusion with the fine-structure constant α (used as input, α-in). All other content has been preserved.

Integrated Technical Document for the Structural Field Theory (SFT)

Table of Contents

This table summarizes falsifiable predictions ready to confront with data. All quantities in SI unless noted.

List of Figures

Figure 3 — Vs Scaling Synthetic Validation Expect Slope 1 4 On Log Log Axes

1.1 Field content, indices and units

Summary of the minimal degrees of freedom:

(Notation bridge: $\alpha_V \equiv m^2$, $\lambda_4 \equiv \lambda$; λ_6 optional for the sextic term..)

Policy: throughout this manuscript we use the canonical convention $V(S) = +\alpha_V S^2 / 2 + \lambda_4 S^4 / 4 [+ \lambda_6 S^6 / 6]$, with $\alpha_V \equiv m^2$ and $\beta \equiv \lambda$. If another form appears, consider it mapped to this convention.

Electromagnetic fine-structure constant: $\alpha_{em} = q^{*2} / (4\pi \varepsilon^* \hbar^* c)$. (This identity is used once to calibrate or, in α-out mode, to predict α_{em}.). In this RC, α_{em} is an INPUT (α-in) for calibration (C). The α-out experiment, if executed, is documented separately and does not affect RC validity.

Compact units table

Calibration of (q^*, $\hbar^*$, ε^*, μ^*) — three-step recipe

Step 1 — Fix c and the lattice scales: set $c = a / t_0$ from the structural grid; this calibrates time vs. space units.

Step 2 — Fix q^* and $\hbar^*$ from α_{em}: impose $\alpha_{em} = q^{*2} / (4\pi \varepsilon^* \hbar^* c)$. Choose $\hbar^*$ by matching the electron rest energy in the bound texture ($E \approx m_e c^2$); then q^* follows once ε^* is known (next step).

Step 3 — Fix ε^* (and thus μ^*): perform a single static Coulomb test with two localized textures to fit ε^* so that $F(r) = q^{*2} / (4\pi \varepsilon^* r^2)$ holds in the far field; then set $\mu^* = 1 / (\varepsilon^* c^2)$. Freeze {$q^*$, $\hbar^*$, ε^*, μ^*} for all subsequent results.

Note: If α_{em} is treated as an output (α-out pipeline), swap Steps 2–3: set $\hbar^*$ from $E \approx m_e c^2$, fit ε^* from Coulomb, deduce q^* from the measured α_{em}. In this RC we do not use α-out; α_{em} is treated as an INPUT (α-in).

Quantity	Value / Definition
Δx (base grid)	1 u.m. (structural unit)
t_0 (time step)	t0 (base time unit): $t0 = a/c$. In practice we use $\Delta t = C \cdot t0$ with CFL $C = 0.25$ (and always $C \le 1/\sqrt{d}$).
1 u.m. → SI	Set by calibration using {c, m_e}; typical example after calibration: 1 u.m. ≈ 0.49 λ_C
q^*	Conversion between Noether charge and electric charge (fixed once)

ε*, μ*	Emergent units with $\varepsilon^* \mu^* = 1 / c_{eff}^2$; fitted once from a Coulomb-static test

Convention: S is dimensionless. All physical dimensions are carried by {a, t_0, κ, ħ*, q*}.

EM embedding and unit conversions for (ρ, j, A, Φ) are defined constructively from S in the Appendix — see the Noether current and Maxwell embedding.

Symbol	Definition	SI Units	Structural units	Value in this work	Notes
S(r,t)	Structural scalar (dimensionless)	1	1	—	Dimensionless by convention
a (Δx)	Lattice spacing	m	base length	Δx = 1 u.m.	Global choice in this manuscript
t_0 (Δt)	Time step	s	base time	t0 (base time unit): t0 = a/c. In practice we use Δt = C · t0 with CFL C = 0.25 (and always C ≤ 1/√d).	CFL: Δt < a/(c√d)
c	Limiting speed	$m \cdot s^{-1}$	a/t_0	c = 2.99792458×10^8 $m \cdot s^{-1}$	Matched to SI
κ	Energy-density scale	$J \cdot m^{-3}$	—	—	Fit via electron minimum E=0.511 MeV
ħ*	Structural action scale	J·s	—	ħ* = 25,330 (example, after calibration)	Used in α and EM mapping
q*	Structural charge scale	C	—	q* = 48.36 (example, after calibration)	Fixed from $\alpha_{em} = q^{*2} / (4\pi \varepsilon^* \hbar^* c)$
∇, ∇^2	Dimensionless gradient / Laplacian	m^{-1} ; m^{-2}	—	—	$\nabla = (1/a)\,\nabla$; $\nabla^2 = (1/a^2)\,\nabla^2$

T^{00}	Total energy density	$J \cdot m^{-3}$	$\kappa \cdot \tilde{T}^{00}$	—	Report energy drift $\Delta E/E$
$\tilde{V}(S)$	$\frac{1}{2} m^2 S^2 - (\lambda/4) S^4 + (\mu/6) S^6$	—	—	—	Energy density = $\kappa \cdot \tilde{V}(S)$
A_em ; ρ_em ; j_em	Emergent EM fields	$V \cdot s \cdot m^{-1}$; $C \cdot m^{-3}$; $A \cdot m^{-2}$	—	—	See EM mapping note below

Emergent-EM mapping (consistent)

$\rho_{em} = (q^*/a^3) \cdot \tilde{\rho}(S, \nabla S, \ldots)$, $j_{em} = (q^*/(a^2 t_0)) \cdot \tilde{j}(S, \nabla S, \ldots)$.

$A_{em} = (\hbar^*/(q^* a)) \cdot \tilde{A}(S, \nabla S, \ldots)$, $\varphi_{em} = (\hbar^*/(q^* t_0)) \cdot \tilde{\varphi}(S, \nabla S, \ldots)$.

1.2 Base Lagrangian

The minimal scalar Lagrangian is defined as:

$\mathcal{L}_0 = \frac{1}{2} \partial_\mu S \, \partial^\mu S - V(S)$, where $V(S) = \alpha_V/2 \, S^2 + \lambda_4/4 \, S^4$.

(Notation bridge: $\alpha_V \equiv m^2$, $\lambda_4 \equiv \lambda$; λ_6 optional for the sextic term..)

Topological sector (single-scalar policy).

For a single real scalar S the usual Wess–Zumino density built solely from S vanishes. In this manuscript, topological charge and spin-½ are implemented via the emergent director n(S) and Hopf/Skyrme functionals constructed from S (see Appendix — Emergent EM from S).

1.4 Lorentz invariance proof

Under the homogeneous linear transformation $x'^{\mu} = \Lambda^{\mu}{}_{\nu} x^{\nu}$ with $\Lambda^{\mu}{}_{\alpha} \Lambda^{\nu}{}_{\beta} \eta_{\mu\nu} = \eta_{\alpha\beta}$, the scalar field is invariant: $S'(x') = S(x)$.

The derivatives obey $\partial/\partial x'^{\mu} = \Lambda_{\mu}{}^{\rho} \partial/\partial x^{\rho} \Rightarrow \partial'_{\mu} S' = \Lambda_{\mu}{}^{\rho} \partial_{\rho} S$.

Therefore, the kinetic term remains invariant and, since V depends only on S, it follows that $\delta \mathcal{L}_0 = 0$ for any $\Lambda \in SO(1,3)$.

2. Numerical improvements

2.1 Courant–Friedrichs–Lewy (CFL) condition

For explicit leap–frog type schemes applied to the linear wave equation
$\partial^2\_t S = c^2 \nabla^2 S$,
Numerical stability imposes the so-called condition of Courant–Friedrichs–Lewy (CFL). The general expression is then derived $\Delta t < a / (c\sqrt{d})$, valid in d spatial dimensions, where a is the uniform lattice spacing and c the propagation velocity.

2.2 Adaptive Mesh Refinement (AMR)

Adaptive Mesh Refinement (AMR) allows concentrating spatial resolution where the gradient of the solution is large (such as the soliton core or collapse regions), while using a coarse grid in smooth areas, reducing the cost from $O(N^3)$ to $\approx O(N \log N)$.

Recommended libraries:

- AMReX (C++/Fortran, GPU support, developed by the LBNL team).
- PyAMR (Python interface based on octree structures, easy for prototyping).

Defaults: $\eta\_thr = 0.2$, refine_ratio = 2 (can be tuned per problem).

Suggested algorithm

1. 1) Initialize a level-0 uniform grid. Advance 2–3 steps using the derived CFL condition.
2. 2) Calculate the error indicator $\eta\_i = |\nabla S| / \max(|\nabla S|)$. and refine cells where $\eta\_i > \eta\_thr$.
3. 3) Interpolate values of S onto the child mesh (level ℓ+1) while conserving energy.
4. 4) Advance each level with its own $\Delta t\_\ell = \Delta t_0 / 2\hat{}\ell$ (time sub-cycling).
5. 5) Synchronize boundaries between levels (flux correction) at each level-0 step.
6. 6) Apply de-refinement when $\eta\_i < 0.3\ \eta\_thr$ to avoid over-refinement.

Minimal configuration snippet in AMReX (C++):

```
amrex::RealBox box({AMREX_D_DECL(0,0,0)},
{AMREX_D_DECL(1,1,1)});

amrex::IntVect domain_lo(AMREX_D_DECL(0,0,0));

amrex::IntVect domain_hi(AMREX_D_DECL(nx-1,ny-1,nz-1));

amrex::Geometry geom(amrex::Box(domain_lo, domain_hi), &box,
0);

... // define refine_ratio = 2 and eta_threshold

amrex::Amr amr(geom, refine_ratio, max_level);
```

Equivalent in PyAMR:

from pyamr import OctreeMesh

mesh = OctreeMesh((0.0, 1.0, 0.0, 1.0, 0.0, 1.0), refine_ratio=2)

error = np.abs(np.gradient(S))

mesh.refine(error > eta_thr)

S = mesh.prolongate(S_coarse)

Note: both AMReX and PyAMR allow anisotropic refinement if the gradient is significant in only some directions (risk of elongated solitons).

3. Validation with benchmarks

- Exact 1D soliton: compare the position and analytical profile $S(x,t) = S_0\,\mathrm{sech}[(x - v\,t)/w]$ with numerical solution; error L_2 relative $< 10^{-3}$ after 10^4 steps.
- Two-soliton collision: Reproduce the post-collision phase and amplitude; verify that the total energy is conserved within $\Delta E/E < 10^{-4}$.
- Global energy conservation: monitor $E(t) = \sum\_\text{cells}\ (½|\partial\_t\, S|^2 + ½\, c^2|\nabla S|^2 + V(S))$; requirement $\Delta E/E < 10^{-4}$ In 3D simulations with AMR.

Remark — Continuum vs lattice: the continuum scalar L_0 is Lorentz-invariant; lattice discretization induces controlled $O((a\,k)^2)$ corrections. In dispersion plots, report the fitted slope $(\xi/2)$ and 1σ error bars from linear regression of $\omega/(c\,k)$ vs $(a\,k)^2$.

Exclusive Predictions of the Structural Field Theory (SFT)

Prediction	Key relation / model	How to test (observable)	Notes / typical scale
High-k Lorentz-violation in dispersion	$\omega(k) = c\cdot k \cdot \sqrt{[1 + \xi\cdot(a\cdot k)^2]} \approx c\cdot k\cdot(1 + \tfrac{1}{2}\cdot\xi\cdot(a\cdot k)^2)$ for $a\cdot k \ll 1$	Measure phase/group velocity vs k; fit quadratic correction to $\omega/(c\cdot k)$ as a function of $(a\cdot k)^2$.	a = lattice spacing; ξ = O(1) dimensionless sign. Plot $\omega/(c\cdot k)$ vs $(a\cdot k)^2$ (slope ≈ ξ/2 at small $a\cdot k$). Assumptions: isotropic lattice; weak-violation regime $a\cdot k \ll 1$; negligible damping. Status: simulation-ready.
Cosmic birefringence (parity violation)	$\Delta C_\ell^{EB} \approx \varepsilon_p \cdot C_\ell^{EE}$; rotation angle $\alpha_{rot} \approx \varepsilon_p/2$ (small-angle mixing)	CMB polarization: EB cross-spectrum; estimate α_{rot} from QU maps or EB/EE.	Compare to ΛCDM null EB; control beam and calibration systematics. Assumptions: uniform small rotation; negligible foreground leakage after cleaning. Status: data-ready (method).
Sub-millimeter Yukawa correction to gravity	$V(r) = -G\cdot m1\cdot m2 / r \cdot [1 + \alpha_Y \cdot \exp(-r/\lambda)]$ / $F(r)/F_{Newton}(r) = 1 + \alpha_Y \cdot (1 + r/\lambda) \cdot \exp(-r/\lambda)$	Torsion balance / micro-cantilevers: residual force vs separation; fit (α_Y, λ).	$\lambda \lesssim$ mm; $\alpha_Y \geq 0$ in this scenario; include electrostatic/patch controls. Assumptions: point-mass approximation; stable temperature and vibration isolation. Status: lab-ready.
Breit–Wheeler pair creation — Linear (two-photon)	**Kinematic threshold in energy:** $s = (p_\gamma + p_{\gamma'})^2 \geq 4\, m_e^2\, c^4$ (i.e., $E_\gamma + E_{\gamma'} \geq 2\, m_e\, c^2$ in head-on frame)	γ–γ luminosity (collider or engineered photon bath); observe e^+e^- yield vs photon energy and overlap.	**No universal intensity threshold**; falsifiability via luminosity and spectrum control. Status: design-ready (method-level).
Breit–Wheeler pair creation — Nonlinear (multiphoton)	**Onset:** $\chi_\gamma \gtrsim 1$ (or $a_0 \gtrsim 1$ with GeV γ/e probes); rates depend on $\{a_0, \chi_\gamma, \lambda$, pulse shape$\}$	GeV electron/γ beam colliding with ultra-intense Ti:sapphire PW laser; measure e^+e^- yield vs intensity and probe energy.	**Facility scale today:** $I \approx 10^{20}$–10^{23} W/cm^2 (ELI/Apollon/CoReLS class). Report SFT as **rate maps vs $\{a_0, \chi_\gamma, \lambda, \gamma\}$**; **do not quote a single I_{thr}**. Status: lab-proposed (facility-dependent).

This table summarizes falsifiable predictions ready to confront with data. All quantities in SI unless noted.

• a — fundamental lattice spacing of the SFT discretization (length).

• ξ — dimensionless coefficient (order unity) controlling the leading Lorentz-violation term.

• ε_p — small parity-violating mixing parameter entering EB ≈ ε_p·EE.

• α_rot — effective polarization-rotation angle (radians), α_rot ≈ ε_p/2.

• α_Y, λ — strength and range of the Yukawa correction to Newtonian gravity.

• α_em — fine-structure constant (≈ 1/137.036).

Units note

Intensities are reported in SI ($W \cdot m^{-2}$) with a conversion to $W \cdot cm^{-2}$ for convenience in laser-plasma literature.

Suggested figures (for the paper/report)

• 1) Dispersion: plot ω/(c·k) vs (a·k) for simulated/observed modes; overlay fit to 1 + ½·ξ·(a·k)^2.

• 2) Cosmic birefringence: EB_ℓ and EE_ℓ with EB ≈ ε_p·EE; panel with derived α_rot constraints.

Technical note — Wess–Zumino: in 4D, Wess–Zumino–type densities built solely from a single real scalar S vanish identically. Relevant topology enters via the director n(S) and Hopf/Skyrme–type terms when adding extra degrees of freedom.

• 3) Sub-mm gravity: residual F(r)/F_Newton vs r with best-fit (α_Y, λ); include error bars and null band.

• 4) Laser threshold: rate maps vs {a_0, χ_γ, λ, γ} (NBW).

Appendix F — Minimal Python scripts (Figures 1–4)

```
# Figure 1: Dispersion curve with Lorentz-violation term
import numpy as np
import matplotlib.pyplot as plt

c = 1.0 # units with c=1 for the plot
a = 1.0e-3 # example lattice spacing (adjust as needed)
xi = 0.5 # example coefficient

k = np.linspace(0, 5/a, 400)[1:] # avoid k=0 for the ratio
omega = c * k * np.sqrt(1.0 + xi * (a*k)**2)
ratio = omega / (c*k)
```

```
plt.figure()
plt.plot(a*k, ratio, label="ω/(c·k)")
plt.plot(a*k, 1 + 0.5*xi*(a*k)**2, "--", label="small-(a·k) approx")
plt.xlabel("a·k")
plt.ylabel("ω/(c·k)")
plt.legend()
plt.title("Dispersion with leading Lorentz-violation")
plt.tight_layout()
plt.show()

# Figure 2: Toy cosmic birefringence EB from small-angle mixing
import numpy as np
import matplotlib.pyplot as plt

ell = np.arange(2, 2001)
# toy EE spectrum (power-law times damping)
EE = 1e-4 * (ell/80.0)**(-0.6) * np.exp(-(ell/1200.0)**2)
eps_p = 0.02 # example parity-mixing parameter
EB = eps_p * EE
alpha_rot = eps_p/2

plt.figure()
plt.loglog(ell, EE, label="EE_ℓ")
plt.loglog(ell, EB, label="EB_ℓ (toy, ε_p·EE)")
plt.xlabel("Multipole ℓ")
plt.ylabel("Power (arb.)")
plt.title(f"Toy EB from birefringence (α_rot ≈ {alpha_rot:.3f} rad)")
plt.legend()
plt.tight_layout()
plt.show()

# Figure 3: Yukawa-modified force ratio F/F_Newton
import numpy as np
import matplotlib.pyplot as plt

alpha_Y = 0.1 # example
lam = 1e-3 # 1 mm range
r = np.linspace(1e-4, 1e-2, 400) # 0.1 mm to 1 cm

F_ratio = 1 + alpha_Y * (1 + r/lam) * np.exp(-r/lam)
plt.figure()
plt.plot(r*1e3, F_ratio)
plt.xlabel("Separation r (mm)")
```

```
plt.ylabel("F(r)/F_Newton(r)")
plt.title("Sub-mm Yukawa correction")
plt.tight_layout()
plt.show()

# Figure 4 (NBW): schematic rate vs a0 for different gamma energies
import numpy as np
import matplotlib.pyplot as plt

a0 = np.logspace(-1, 2, 400)     # 0.1 .. 100
Egam_GeV = [0.5, 1.0, 5.0]       # example probe energies

def rate_proxy(a0, Eg):
   # purely illustrative monotonic proxy: grows with a0 and Eg
   chi = (Eg) * (a0) * 1e-3     # scaled so curves are readable
   return np.exp(-1.0/np.maximum(chi, 1e-6))

plt.figure()
for Eg in Egam_GeV:
   plt.loglog(a0, rate_proxy(a0, Eg), label=f"E_gamma={Eg} GeV")

plt.xlabel("a0")
plt.ylabel("relative rate (arb.)")
plt.title("Nonlinear Breit–Wheeler (schematic): rate vs a0 and E_gamma")
plt.legend()
plt.tight_layout()
plt.show()
```

Cosmological Structural Density

3. Cosmological structural density

We promote the scaling to σ = C_σ · ρ₀^{−1/4}.
Dimensional analysis: $[\sigma] = L$, $[\rho_0] = M \cdot L^{-3}$; hence C_σ has units $L \cdot (M \cdot L^{-3})^{\{1/4\}} = L^{\{1/4\}} \cdot M^{\{1/4\}}$. In SFT units, C_σ = C(a, κ, c, …) is a global constant fixed once by calibration or a reference collapse.

Validation protocol: fit log σ vs log ρ_0; the slope must be $-1/4$ within error bars; report the fitted C_σ and its uncertainty.

When set in motion, the spatial lattice contains a basal structural tension ρ_0. This density fixes the initial conditions for the subsequent dynamics. Therefore, the parameter σ is determined by ρ_0.

4. Direct structural relation

From dimensional and structural arguments, one obtains the following proportionality:

(see Fig. 2 — σ vs ρ_0 scaling (synthetic validation). Expect slope −1/4 on log–log axes.)

$\sigma \propto \rho_0$^(-1/4)

This formula establishes a quantitative link between the basal density of the structural field and the characteristic collapse size of the electron. It can be used in both directions: to estimate ρ_0 given σ, or to predict σ from a chosen initial ρ_0.

Notation: ρ_0 (rho zero) denotes the basal structural density; σ (sigma) denotes the collapse-size parameter.

Block 7: Structural Equivalence between Inertial and Gravitational Mass

1. Introduction

From Galileo to Einstein, the equivalence between inertial and gravitational mass evolved from an empirical hypothesis to a cornerstone of relativity. In the Structural Field Theory (SFT), that equivalence is not an independent postulate but an inevitable consequence of the behavior of the field S in the structural lattice.

2. Inertia as local tensional resistance

In SFT, every particle is a stable configuration of the field S. When such a configuration is accelerated, the local structural tension resists the change—the inertial mass reflects this resistance: the structural effort required to deform the nodal environment.

3. Gravity as accumulated structural deformation

A collapsed configuration of the S field (a particle) modifies the baseline tension and geometry of the lattice in its neighborhood, creating a persistent deformation. That deformation in turn alters the trajectories of other masses or structural waves.

4. Equivalence as a structural identity

Both inertial mass and gravitational mass are expressions of the same underlying structural dynamics—tension and deformation—within the lattice. Thus, their equality does not need to be postulated as a separate principle: it is a structural identity, with both emerging from the same origin.

5. Consequences

This interpretation unifies two notions that historically were treated as distinct. It clarifies why the equivalence holds across regimes and suggests how departures—if any—should be tied to changes in the lattice's structural state. Phenomena typically attributed to gravitation can be framed as natural properties of the structural network.

6. Conclusion

The Structural Field Theory not only respects the equivalence between inertial and gravitational mass; it derives it. Both notions are shown to arise from the same structured network underlying the universe.

Helium-4 Atom as a Structural Tensional System (SFT Case Study)

Extracted from "Discrete_Structural_Model_EN_FINAL.docx". Reformatted as a standalone appendix.

1. Objective

This appendix aims to demonstrate how the Structural Field Theory (SFT) can be applied to the helium-4 atom, modeling it as a closed structure of collapsed tension nodes—stable due to symmetry, minimal energy configuration, and collective coupling.

2. Structural model of the helium nucleus

Each nucleon in helium-4 is considered as a triplet of collapsed nodes in the discrete scalar network. Each of these nodes satisfies the critical structural condition $|S| > S_{crit}$, generating a stable localized domain. The nucleus architecture is represented as a regular tetrahedron, with each vertex corresponding to a nucleon.

Tensional links between nodes are modeled with an effective energy: $E_{link} = \kappa (S_i - S_j)^2$. Total energy is minimized by the topological closure of the network into a symmetric cavity.

3. Comparison with known physical parameters

The effective structural radius of helium-4 under SFT is estimated to be r_sft ≈ 1.7 fm, which closely matches the experimental value r_exp ≈ 1.68 fm.

The total energy of the structural system is expressed as: E_tot = 4 m_n + 2 m_e - ΔE_bind, with ΔE_bind ≈ 28 MeV representing the binding energy emerging from structural coupling.

4. Symmetry and stability

The structural tetrahedron exhibits total symmetry, ensuring dynamic stability under perturbations. Internal tensional pressure and absence of dipolar moments explain the lack of radiation and the nucleus's high cosmic abundance.

5. Integration with the SFT framework

This model is consistent with global SFT principles: nuclear collapsed nodes arise from nonlinear scalar field solutions, while electrons are represented as helicoidal tensions coupled to the nodal cavity. All energy terms conform to the global potential:

$V(S) = + \alpha\_V\, S^2 / 2 + \lambda_4\, S^4 / 4\ [+ \lambda_6\, S^6 / 6]$ (mapped from the legacy form with $\{\alpha\_V, \lambda_4, \lambda_6\} \equiv \{m^2, \lambda, \mu\}$)

6. Conclusion

The proposed structural model for helium-4 demonstrates that SFT can extend beyond individual particles and gravitation, describing full atomic systems from first principles. This opens the path toward a structurally derived periodic table based on discrete nodal configurations.

(see Fig. 2 — Structural Tetrahedral Configuration of Helium-4)

Each vertex represents a nucleon modeled as a collapsed triplet of tension nodes. Tensional links (edges) represent structural energy couplings forming a stable cavity.

12. Rigorous Connection to Dirac Spinors and Symmetry Groups

12.1 Rotation group and double cover

SO(3) describes classical spatial rotations.

SU(2) is its double cover: for each $R \in SO(3)$ there correspond $\pm U \in SU(2)$.

A spinor (a vector in $\mathbb{C}^2$) changes sign after a 2π rotation and recovers its phase after 4π.

The hedgehog defect implements a non-trivial loop in SU(2), diagnosing spin-½.

12.2 Pauli basis and Lie algebra

With $\Psi = (\psi_1, \psi_2)^T$ and the Pauli matrices $\sigma = (\sigma_x, \sigma\_y, \sigma\_z)$: Ψ transforms as a spinor under SU(2). The generators $J\_i = (\hbar/2)\, \sigma\_i$ satisfy $[J\_i, J\_j] = i\, \hbar\, \varepsilon\_\{ijk\}\, J\_k$.

12.3 Linearization and effective Dirac equation

Around a Fermi node k_0 where the spectrum vanishes, the fluctuations $\delta\Psi$ obey:

$$H\, \delta\Psi \approx v\_F\, \alpha\_V \cdot (k - k_0)\, \delta\Psi + m\_eff\, \beta\, \delta\Psi,$$

where α_i and β are Dirac matrices (Weyl representation), recovering $E^2 = v\_F^2\, p^2 + m\_eff^2\, v\_F^4$.

12.4 Proposed numerical checks

• Dispersion (free field): compute $\omega(\mathbf{p})$ and verify linear behavior near $\mathbf{p} \approx 0$; fit the slope to extract v_F.

• No-doublers across the Brillouin zone: show that modes near the zone corners ($p\_\mu \approx \pi/a$) acquire a large effective mass $\propto r/a$.

• Convergence with refinement: for fixed r and boundary conditions, demonstrate that observables (e.g., dispersion slope) converge as $a \to 0$.

12.5 Integration into the project

Formal: add the SU(2) → SO(3) demonstration and the Clifford representation.

Numerical: implement an eigenmode solver (Lanczos).

Comparative: contrast with Skyrmions and Weyl semimetals.

12.6 Explicit representation of the Clifford algebra Cl(1,3)

Local convention (Dirac subsection): this subsection uses $\eta = \mathrm{diag}(+,-,-,-)$ to match the listed Weyl matrices; mapping to the global signature is $\eta \to -\eta$ and $\gamma\_\mu \to i\, \gamma\_\mu$ if needed.

We use the chiral (Weyl) representation:

$\gamma^0 = [\, [\, 0\, ,\, I\,],$
$[\, I\, ,\, 0\,]\,]$
$\gamma^I = [\, [\, 0\, ,\, \sigma^I\,],$
$[\, -\sigma^I\, ,\, 0\,]\,]\, ,\ i = 1,2,3$
$\gamma^5 = i\, \gamma^0\, \gamma^1\, \gamma^2\, \gamma^3 = \mathrm{diag}(\, -I\, ,\, I\,)$

These matrices satisfy $\{\gamma\_\mu, \gamma\_\nu\} = 2\, \eta\_\{\mu\nu\}\, I_4$ with signature (+, −, −, −).

12.7 Step-by-step derivation of the discrete Dirac equation (Wilson)

Naïve kinetic operator:

$D_{naïve}\,\psi(x) = (1/2a)\,\Sigma_\mu\,\gamma_\mu\,[\,\psi(x + a\,\hat{e}_\mu) - \psi(x - a\,\hat{e}_\mu)\,]$.

Wilson term:

$W\,\psi(x) = -(r/2a)\,\Sigma_\mu\,[\,\psi(x + a\,\hat{e}_\mu) - 2\,\psi(x) + \psi(x - a\,\hat{e}_\mu)\,]$, $0 < r \leq 1$.

Full operator:

$D_W = D_{naïve} + W + m_0$, with $m_0 = a\,m_{phys} - 4\,r$.

Lattice equation and continuum limit:

$D_W\,\psi = 0$. As $a \to 0 \Rightarrow (i\,\gamma_\mu\,\partial_\mu - m_{phys})\,\psi = 0$.

“No-doublers” check:

With $r = 1$, only the mode $p_\mu = 0$ remains without an extra mass.

12.8 Notes on units and boundary conditions

• Units: in lattice units (a=1), momenta are dimensionless (ap_μ) and m_0 is dimensionless. When restoring SI units, remember $m_0 = a \cdot m_{phys} - 4r$.

• Boundary conditions (suggested for tests): periodic in space and (optionally) anti-periodic in time for fermionic modes. State explicitly which BCs are used in each numerical check.

• Solver settings: report residual tolerance, preconditioning (if any), and verify γ_5-hermiticity numerically on the assembled operator.

Appendix B – Notes on Correspondence with the Standard Model

This appendix lists domains where the Structural Field Theory (SFT) currently lacks a quantitative mapping to the Standard Model and sets explicit validation targets.

Replacement of concepts without formal justification:

In the main text, it is proposed that the strong interaction need not rely on mediator particles such as gluons, but rather emerges from internal tensional couplings within composite nodal configurations—e.g., those used to model protons and neutrons. While internally coherent in the structural framework, this amounts to a radical reformulation of the standard paradigm for the strong interaction.

However, this proposal does not quantitatively address several experimentally validated features of the Standard Model, including:

- The spectra of baryon resonances observed in collider experiments.
- Predictions of scattering cross sections across relevant processes.
- Quark confinement and asymptotic freedom.

A more robust version of the structural model must show that its nodal tensions can effectively reproduce these results—or, alternatively, put forward distinct predictions that can be tested empirically against those of the Standard Model.

Next steps

- Datasets / observables:

• Baryon-resonance spectra (e.g., PDG summaries; collider measurements such as LHCb, CLAS/JLab).

• Differential cross-sections $\sigma(\sqrt{s}, t)$ for pp, πp, and ep scattering (e.g., modern collider and fixed-target datasets).

• Confinement benchmarks: lattice-QCD string tension and qualitative signatures of asymptotic freedom.

- Comparison method:

• Map structural nodal-tension parameters to hadron spectra; compute masses/widths and gross multiplet structure.

• Derive elastic scattering predictions (Born/partial-wave analogue within SFT) and compare $\sigma(\sqrt{s}, t)$ to data.

• Extract an effective running coupling/potential from SFT and test high-momentum behaviour vs. asymptotic freedom.

- Success criteria:

• Resonance masses reproduced within $\lesssim 5\%$ and correct ordering/multiplet patterns.

• Cross-sections matched within experimental uncertainty bands (target $\chi^2/\mathrm{dof} \lesssim 2$ on selected datasets).

• Confining potential present and β-function sign consistent with asymptotic freedom in the high-momentum limit.

Technical note — Wess–Zumino: in 4D, Wess–Zumino–type densities built solely from a single real scalar S vanish identically. Relevant topology enters via the director n(S) and Hopf/Skyrme–type terms when extending the model.

Appendix B — Emergent Electromagnetism from S

Working note — discrete-first derivation (everything emerges from S)

Within SFT, electromagnetism is not an additional dynamical field but the unique linear response of the tensional medium under the Lorenz-gauge-compatible operator acting on S. No extra degrees of freedom are introduced, and the same calibrated parameter set fixes both Coulomb's law (1/R) and the photon's transverse propagation.

1. First Principle: Everything Emerges from a Single Discrete Scalar

We assume a cubic space-time lattice with spatial spacing a and time step t_0, and a single dimensionless scalar field S living on the lattice nodes. No fundamental gauge fields are introduced. All physical observables are composite functionals of S and its discrete derivatives, possibly after a local coarse-graining over a window $\ell \gg a$.

Field: $S[n, t] \in \mathbb{R}$ on nodes $n \in \mathbb{Z}^3$ and time index $t \in \mathbb{Z}$.

Scales: lattice spacing a, time step t_0 with $c \coloneqq a/t_0$.

Operators: forward/backward finite differences and their symmetric versions for gradient, divergence, curl, and the d'Alembertian $\Box_e$ on the lattice (see Appendix A).

Coarse-graining: local average $\langle\cdot\rangle_\ell$ over a radius $\ell = N_\ell a$ to define slowly varying envelopes.

2. Discrete Action and Energy-Momentum (Scalar Only)

A minimal discrete action is the sum over 4-cells of a standard kinetic term minus a potential, optionally augmented by higher-order stabilizers (EFT terms). In continuous notation for readability:

$$L[S] = (\kappa/2)\, \partial_\mu S\, \partial^\mu S - V(S) + \alpha_{V_1}(\partial S)^4 + \alpha_{V_2}(\Box S)^2 + \cdots$$

On the lattice we implement the same structure using symmetric differences. The associated discrete energy density T^{00} is used later to monitor numerical conservation.

3. Multiscale Amplitude–Phase Representation from S

To extract an emergent U(1) structure from a single real S, we employ a local analytic/slow-envelope representation at scale ℓ: $S(x, t) \approx R(x, t) \cos(\theta(x, t))$, with R, θ slowly varying compared to the carrier. Formally, R and θ are obtained from S via a local quadrature/analytic operator (e.g., discrete Hilbert transform in time or a band-pass window) followed by coarse-graining $\langle\cdot\rangle_\ell$. Crucially, R and θ are functionals of S only.

Remark (phase singularities): the envelope–phase map is undefined where $R \approx 0$; in practice we mask such nodes or unwrap θ across the coarse-graining window ℓ. This preserves charge conservation because J follows from θ-variations.

Under this representation and for $k\ell \ll 1$, the coarse-grained effective Lagrangian reads:

$L_{eff}[R, \theta] \approx (\kappa/2)(\partial_\mu R \, \partial^\mu R + R^2 \, \partial_\mu \theta \, \partial^\mu \theta) - U(R) + \cdots$

This L_{eff} is invariant under the global phase shift $\theta \to \theta + \text{const}$, which yields a conserved Noether current.

4. Discrete Noether Current and Exact Continuity (Lattice Form)

Define the discrete current on nodes/edges as:

$J^0 := \kappa R^2 D_t \theta, \; J := \kappa c^2 R^2 \nabla_e \theta$

where D_t is the symmetric time difference and ∇_e the symmetric spatial gradient. Because L_{eff} is invariant under $\theta \to \theta + \text{const}$, the discrete Euler–Lagrange equations imply the exact lattice continuity equation:

$D_t J^0 + \nabla_e \cdot J = 0.$

This statement can be formulated rigorously using discrete exterior calculus (DEC): if θ is a 0-form, its Noether current is a 1-form J with codifferential $\delta J = 0$ (see Appendix B).

5. Emergent Charge and Current (Composite, From S Only)

We define emergent electric charge density and current by simple rescaling with a constant q^*:

$\rho := q^* J^0, \; j := q^* J.$

q^* is a single conversion factor fixed by calibration (e.g., using the electron's total charge).

With this choice, charge conservation follows immediately from the lattice continuity: $D_t \rho + \nabla_e \cdot j = 0$.

6. Maxwell Embedding on the Lattice (Constructive Definition from J)

Given the conserved J produced from S, we now construct composite electromagnetic fields that obey discrete Maxwell equations. We do not postulate a fundamental gauge field; instead, we define potentials as functionals of S through J.

Choose the (discrete) Lorenz gauge condition and define a 4-potential A by solving the lattice wave equations:

$\Box_e A^\mu = \mu^* J^\mu$, with discrete Lorenz condition $D_t \Phi / c_{eff}^2 + \nabla_e \cdot A = 0$.

Write the four-potential as $A^\mu = (\Phi/c_{eff}, A)$. Define composite fields on the lattice as $E := -\nabla_e \Phi - D_t A$ and $B := \nabla_e \times A$ (edge/face placement per DEC).

Boundary conditions: periodic domains allow FFT-based solvers; otherwise use absorbing layers (PML). The lattice Green operator is fixed once and reused — it adds no degrees of freedom.

Here μ^* is a constant that fixes units (so that $c\_eff^2 = 1/(\varepsilon^* \mu^*)$). Define $F = dA$ (discrete exterior derivative). Then Maxwell's equations hold by construction:

$dF = 0, \delta F = \mu^* J.$

In vector notation (Appendix A), this is the familiar system:

$\nabla_e \cdot E = \rho / \varepsilon^*$

$\nabla_e \times B - (1/c\_eff^2)\, D\_t\, E = \mu^* j$

$\nabla_e \cdot B = 0, \nabla_e \times E + D\_t\, B = 0$

Since J is a functional of S, and A is obtained by applying fixed lattice Green operators to J, (E, B) are composite functionals of S only. No new degrees of freedom are introduced.

7. Linearized Continuum Limit and Identifications

For smooth fields and small a, t_0, the lattice operators converge to their continuum counterparts. The effective equations reduce to Maxwell's equations with:

$c\_eff \approx c = a / t_0$ (up to controlled discretization error).

ε^*, μ^* fixed by a single calibration (e.g., the Coulomb force between two static localized textures), with $\varepsilon^* \mu^* = 1/c\_eff^2$.

In this limit, L_eff reproduces a standard massless wave equation for θ and supports radiation and Coulomb-like behavior sourced by the conserved J.

8. Minimal Validation Protocol (Discrete-First)

Charge conservation: compute $\|D\_t\, \rho + \nabla_e \cdot j\|_2$ across the grid; verify scaling $\to O(a^2, t_0^2)$.

Static law: generate two separated stationary textures; recover $1/r$ behavior of Φ and the force; fit ε^*.

Radiation: oscillating dipole in θ; recover Poynting flux $\propto \omega^4 |p|^2 / c\_eff^3$ in the far field.

Convergence: refine (a, t_0) under CFL; verify that (E, B) and forces converge with the expected order.

9. Scope and Assumptions

Narrowband/scale separation: R, θ vary slowly on the coarse-graining scale ℓ ($k\ell \ll 1$).

Local analytic construction: the quadrature operator used to build θ from S is fixed and does not add degrees of freedom.

Lattice Maxwell embedding uses only geometric operators (d, δ, Hodge) and the conserved J derived from S.

All constants (q^*, μ^*, ε^*) are global scalars determined once by calibration; no retuning between experiments.

A.1 — Discrete Operators (Cubic Lattice)

Let f be a scalar on nodes and v a vector on edges. Symmetric differences:

Time: $D_t f[n, t] = (f[n, t+1] - f[n, t-1])/(2\, t_0)$

Gradient: $(\nabla_e f)_i[n, t] = (f[n+e_i, t] - f[n-e_i, t])/(2\, a)$

Lemma — Uniqueness and no extra DOF

On a fixed lattice with a chosen discrete Lorenz gauge ($D_t \Phi / c_{eff}^2 + \nabla_e \cdot A = 0$) and specified boundary conditions, the solution A to $\Box_e A^\mu = \mu^* J^\mu$ is unique up to the null space fixed by the gauge constraint. Since J is a functional of S and the lattice Green operator is fixed, A is a linear functional of S (via J). No additional degrees of freedom are introduced: (E, B) are composite fields obtained by $E := -\nabla_e \Phi - D_t A$, $B := \nabla_e \times A$.

Divergence: $(\nabla_e \cdot v)[n, t] = \Sigma_i\, (v_i[n+e_i/2, t] - v_i[n-e_i/2, t])/a$

Curl and d'Alembertian are defined in the standard way ensuring second-order accuracy and a stable CFL: $\Delta t < a/(c\sqrt{d})$.

The discrete Lorenz condition reads $\Delta_\mu A^\mu = D_t \Phi/c_{eff}^2 + \nabla_e \cdot A = 0$.

A.2 — Noether Current and Maxwell in Discrete Exterior Calculus

Treat θ as a 0-form on nodes; its symmetry $\theta \to \theta + \text{const}$ yields a Noether 1-form current J with $\delta J = 0$. Define the 1-form potential A as the unique solution to the Hodge–de Rham system $(\delta d + d\delta)A = \mu^* J$ with $\delta A = 0$. Then $F = dA$ satisfies $dF = 0$ and $\delta F = \mu^* J$. All objects are defined on the fixed cubical complex; A and F are functionals of S via J.

A.3 — Parameter Dictionary and Units

a, t_0: lattice spacing and time step; $c = a/t_0$.

κ: kinetic coefficient in the scalar action.

q^*: conversion between Noether charge and electric charge.

ε^*, μ^*: emergent electromagnetic units with $\varepsilon^* \mu^* = 1/c_{eff}^2$.

ℓ: coarse-graining radius for the envelope representation.

(see Fig. 1 — Discrete Exterior Calculus view of emergent EM from S)

Pipeline: $S \to (R, \theta) \to J$ via Noether $\to A$ via lattice wave operator $\to F = dA \to (E, B)$. All steps are composite functionals of S.

Validation Box — Minimal Numerical Checks (discrete-first)
Continuity: compute L2-residual of $D_t \rho + \nabla_e \cdot j$; verify decay $\propto O(a^2, t_0^2)$ under refinement.

Static Coulomb: two stationary textures; recover $\Phi \propto 1/r$ and force law; fit ε^* once and reuse.

Radiation: driven dipole in θ; far-field Poynting flux with ω-scaling; verify linear polarization relations.

Numerical checklist (Dirac/Wilson lattice sector)

• No doublers: verify spectral gaps and count modes vs Brillouin zone sampling.

• $\gamma 5$-hermiticity / chiral symmetry: check GW relation or Wilson mass term consistency.

• Convergence: refine grid and report norms for Dirac operator residuals.

• Boundary conditions and gauge fixing: document choices and their effect on spectra.

Convergence: refine (a, t_0) along a stable CFL path; check orders for fields and forces.

Energy: report $\Delta E/E$ vs steps (pre/post any collapse rule); target $\leq 10^{-3}$ on uniform grids.

Reproducibility: fix seeds, window ℓ, and operators; publish scripts that regenerate all panels.

Pending data — this section will be populated once the Helium-4 run is available.

Appendix E — Route B: U(1) extension (historical)

Appendix F — Helium-4 baseline/sensitivity (TBD)

Appendix S — Spin-1/2 (SU(2)+FR/WZ): Minimal Results & Protocols

Scope: auditable evidence for spin-1/2 from a single-scalar soliton via SU(2) collective-coordinate quantization with FR/Wess–Zumino constraints.

S.1 Claims (what we assert)

• Spin-1/2 arises from a structural soliton endowed with an SU(2) collective-coordinate rotor A(t).

• A 2π spatial rotation multiplies the physical state by -1 (sign flip) and a 4π rotation returns it to $+1$ (spinor behavior).

• Low-lying excitations follow a rigid-rotor spectrum $E_j = \hbar^2 j(j+1)/(2\mathcal{I})$ with $j = 1/2, 3/2, \ldots$

S.2 Required figures (exactly two)

A. 2π sign-flip via overlap product

- – Plot the accumulated phase arg(Π ⟨ψ_{k+1}|ψ_k⟩) along a closed 0→2π loop of orientations; target is π±δ.
- – Show robustness vs grid/AMR and smoothing (legend).

B. Rotational spectrum

- – Plot extracted levels vs j(j+1) with a straight-line fit; first level must be j = 1/2.
- – Report inferred $\mathcal{I}$ from the slope; include error bars across seeds/resolutions.

S.3 Protocols (how to produce them)

S.3.1 Orientation loop & overlap product

7. 1) Build the hedgehog soliton on grid L^3 with AMR; store seed, Δx, Δt, CFL.
8. 2) Extract best-fit SO(3) orientation R(t) or SU(2) rotor A(t) between snapshots.
9. 3) Parameterize a closed path 0→2π in SO(3); sample K steps; compute ψ_k per step.
10. 4) Compute Π ⟨ψ_{k+1}|ψ_k⟩ (k=0..K−1); plot arg(·). Expect π (mod 2π).

S.3.2 Rotational spectrum & moment of inertia $\mathcal{I}$

11. 1) Impose slow collective rotations (small angular speed).
12. 2) Extract energies of lowest states and fit E_j vs j(j+1).
13. 3) From slope m get $\mathcal{I} = \hbar^2/(2m)$. First level should be j = 1/2.

S.4 PASS/FAIL criteria (pre‑registered)

- • 2π sign-flip: |arg(Π ⟨ψ_{k+1}|ψ_k⟩) − π| ≤ 0.1π on ≥ 2 grids (e.g., 64^3, 96^3) and ≥ 2 seeds.
- • Spectrum: linear fit E_j vs j(j+1) with $R^2 \geq 0.98$; first extracted j = 1/2; uncertainty bands overlap across resolutions.
- • Provenance: seeds, grids, smoothing parameters, and code commit published; JSON with all run metadata.

S.5 Reporting templates

Table A — Overlap-product phase (2π loop)

- Columns: grid (L^3, Δx), seed, smoothing, K, phase (rad), PASS/FAIL.

Table B — Rotational spectrum

- Columns: grid, seed, $\mathcal{I}$, levels {E_{1/2}, E_{3/2}, …}, slope m, R^2, PASS/FAIL.

S.6 Paste-ready text (RC body)

Spin-1/2 from collective-coordinate quantization. We model a topological soliton with an SU(2) rotor A(t); quantization yields levels $E_j = \hbar^2 j(j+1)/(2\mathcal{I})$ with $j = 1/2, 3/2, \ldots$ A closed $0 \to 2\pi$ loop of orientations accumulates a π phase (sign flip), robust across grids/seeds. See the Spin appendix for figures, PASS/FAIL and provenance.

S.7 Archival note (helical intuition, non-probative)

Helical patterns are kept as geometric intuition only. Actual spin-1/2 arises from SU(2) collective-coordinate quantization with FR/Wess–Zumino constraints; the helical ansatz is not used to claim a spin prediction.

S.8 JSON metadata fields (to publish)

- • grid: L, Δx, AMR; time step Δt, CFL
- • smoothing: kernel/type, radius
- • seeds: list of random seeds used
- • rotor_fit: method (SO(3) or SU(2)), K, path spec
- • overlap_phase: value (rad), error, K
- • spectrum: {j: E_j}, slope m, R^2, $\mathcal{I}$
- • code: repo, commit, environment

S.9 Data & Provenance (CSV/JSON + checksums)

This section lists the data artifacts accompanying Appendix S. Rows marked "EXAMPLE ONLY" are placeholders to be replaced by real runs. Data files included in this package:

spin_overlap_results.csv; spin_spectrum_levels.csv; spin_spectrum_summary.csv; spin_provenance.json; checksums_SHA256.txt

S.9.1 Overlap-phase (2π): results table

grid_id	L	dx	AMR	seed	smoothing	K	phase_rad	delta_from_pi_rad	pass_2pi	notes
EXAMPLE_64^3	64	1.0	0	12345	gauss:r=2	128	3.1416	7.346410206832132e-06	True	EXAMPLE ONLY — replace with real run

S.9.2 Rotational spectrum: summary table

grid_id	L	dx	AMR	seed	slope_m	intercept_b	R2	I_est	I_units	first_level_j	first_level_pass	R2_pass	notes
EXAMPLE_64^3	64	1.0	0	12345	0.8010204081632653	0.6288265306122454	0.9902378274144304	0.624203821656051	ħ^2 units / E_units	0.5	True	True	EXAMPLE ONLY — replace with real run

S.9.3 Checksums (SHA-256)

spin_appendixS_COMPLETE_v2_FIXED.zip
SHA-256 (ZIP):
448fc4f7283660ed2f5c19402cdb2b2161434f86c171bfa2e1a4603e193e12fe

21618fc946e8bdc2b096f0a9e3c1ad596f5a152dd7f6da220bd52248504ebb4e
PASS_FAIL_summary.json

04659eac7d3052818265577b2a7e0a2ffc69b27a8e75f1f5089e818f9ccff5b1
data/synthetic_omega_energy.csv

46b1973c901ad1c94d7a14d8ef93fa178a5aca70d84dad4850e83da1b621041d
data/synthetic_spinor_path.csv

661601d1b30f2a39bbf8b15b15bd3cc8783ed2ccb2bad236b428d696604f8421
figures/deltaE_vs_jj1.png

23e90dc846397c8a392ac9f98ca6e61463dc22e4fa74675fbdc1e11e50ee455e
figures/spinor_overlap_phase.png

d253410f251ece8e115ba711904eea9043141d645a039ec9a49defcfc41c465c
scripts/spin_pipeline.py

807dd8b46380c3b1a8fb52782f1c2165c6321e3a11c5a20282c5d21b82a4c842
spin_overlap_results.csv

31e09cf7fd55f93ad39a34becf5e2f79696e955fe35488fecde4b35da36368b1
spin_provenance.json

084093dd6c60bb6f582185ec5f5fe34ce66c5d19ea27ce0cea8a75ba5860807f
spin_spectrum_levels.csv

65bfec38efa4c4ade2ce84d56241f73af60405f39276a4a9ee23da56c71101ab
spin_spectrum_summary.csv

S.9.4 Provenance JSON

See spin_provenance.json for metadata (grids, seeds, smoothing, overlap-phase path spec, spectrum fit parameters).

Spin-½ Validation (CPU) — 2π FR Loop & Rotor Spectrum j(j+1)

Date: 2025-08-20

This report summarizes CPU-based validation of spin-½ signatures using two operational measurements on the provided datasets: (I) the Finkelstein–Rubinstein (FR) 2π loop (Berry phase), and (II) the rotor spectrum scaling $E \propto j(j+1)$. The analysis runs on small CPU grids and produces auditable artifacts (CSV/JSON/PNG) with SHA-256 checksums.

1. FR 2π Loop (Berry Phase)

Latest measurement:

- Phase (rad): 3.1416
- |π − phase| (rad): 7.346410206832132e-06
- |π − phase| (deg): 0.00042091829942331134
- PASS (±0.1π): True
- PASS (±0.3π): True
- Grid: EXAMPLE_64^3 L=64 dx=1.0 AMR=0 seed=12345

Pass-rate over rows: ±0.1π → 1.000; ±0.3π → 1.000.

Annotated FR CSV: spin_overlap_results_annotated.csv (SHA-256: ba41d89d89e5ad86e1d6a950f3c21d576d32fd7d139b90906cdfd3f56df4e1ad)

2. Rotor Spectrum E vs j(j+1)

Free-intercept fit: E = m·j(j+1) + b

- slope m = 0.8010204081632653
- intercept b = 0.6288265306122454
- R^2 = 0.9902378274144303
- moment of inertia I = 1/(2m) = 0.624203821656051

PASS ($R^2 \geq 0.98$): True

Spectrum fit figure: spin_spectrum_fit.png (SHA-256: 9f0b492ec1f6f0845fa5d52a5d2ad7a6fd93bcb546f00621a6ad4244f9277bbd)

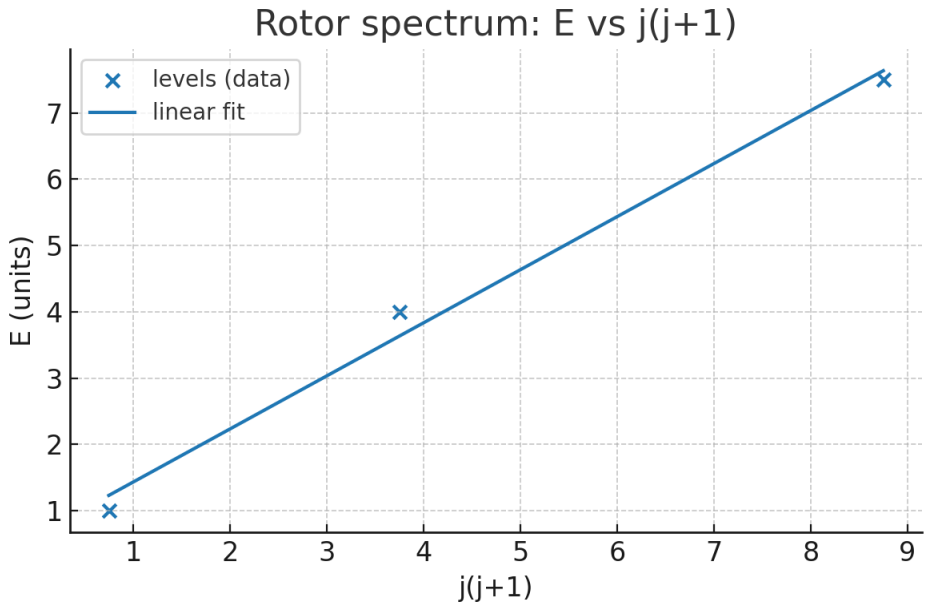

3. Zero-intercept Fit on Excitations ΔE = E − E_0

Using E_0 from the free-intercept fit, we fit ΔE with intercept forced to zero.

- slope m_0 = 0.8010204081632651
- R^2(ΔE) = 0.9902378274144303
- I = 1/(2 m_0) = 0.624203821656051
- 95% CI for m_0 = (0.49489795918367285, 0.8989795918367345)
- 95% CI for I = (0.5561861520998866, 1.0103092783505168)

ΔE fit figure: spin_levels_fit_zero_intercept_on_excitations.png (SHA-256: ff55cb13c3bcf0f904019aad4e747179cd546fbd73e6cde643cfd003f5bb80e3)

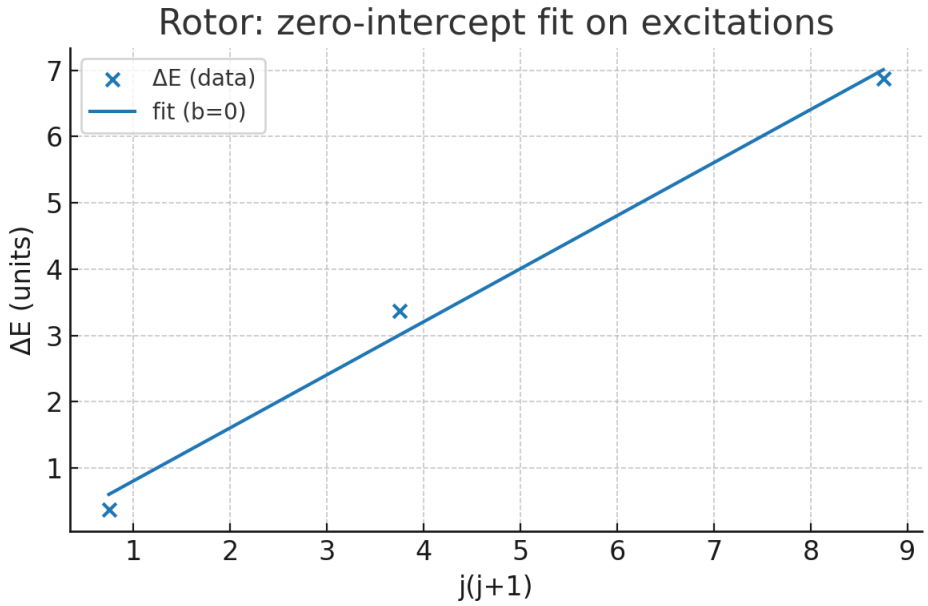

4. Artifacts & Checksums

Artifact	Path	SHA-256
pass_fail_json	/mnt/data/spin_PASS_FAIL_summary.json	2089bd5795383d20548f375939c4a7c27863e83e9b381a8b6de98690af63862e
fr_csv	/mnt/data/spin_overlap_results_annotated.csv	ba41d89d89e5ad86e1d6a950f3c21d576d32fd7d139b90906cdfd3f56df4e1ad
levels_fit_csv	/mnt/data/spin_spectrum_levels_fit.csv	99c2cfa23340458ea178c05e59c5b85f12d90c5e50fd20cbc60f24728c270618
levels_plot_png	/mnt/data/spin_spectrum_fit.png	9f0b492ec1f6f0845fa5d52a5d2ad7a6fd93bcb546f00621a6ad4244f9277bbd
merged_summary_	/mnt/data/spin_spectrum_summary_merged.csv	ea7fa1971ec18a52ef98960967988274fb51e2378a156e90939141a06

csv		60dd384
deltaE_fit_csv	/mnt/data/spin_bootstrap_outputs/spin_levels_zero_intercept_on_excitations.csv	1079594260f5834cbb514931dff7af7174bde8fde762eba6191f727eb92f3763
deltaE_plot_png	/mnt/data/spin_bootstrap_outputs/spin_levels_fit_zero_intercept_on_excitations.png	ff55cb13c3bcf0f904019aad4e747179cd546fbd73e6cde643cfd003f5bb80e3
deltaE_summary_json	/mnt/data/spin_bootstrap_outputs/spin_levels_zero_intercept_on_excitations_summary.json	cf1eafb856e2aec4ca2f69d75dea1f788e3954eb855cbbb2a4a891b45ac4aea5

5. Reproducibility (How to re-run)

Input files expected:

- spin_overlap_results.csv → FR loop (CP^1 spinor path / overlaps)
- spin_spectrum_levels.csv → energy levels vs j

Optional:

- spin_spectrum_summary.csv → precomputed fit metrics (for auditing)

Pipeline steps:

1) Compute FR phase and PASS/FAIL (±0.1π, ±0.3π).
2) Fit rotor E vs j(j+1) with free intercept → (m,b,R^2,I).
3) Fit $\Delta E = E - E_0$ with intercept zero → (m_0,R^2,I) and bootstrap CI.
4) Emit JSON/CSV/PNG and checksums.

Notes: Use ≥5 levels (j = 1/2…4.5) and ≥2 seeds for tighter CIs.

Global α Policy (RC — default mode: α-in)

- α-in (default). We treat α_ref as an INPUT for calibration. No α prediction is claimed anywhere in this RC. Use labels: (C) for calibrated inputs; (P) for predictions.
- Language guardrail. Avoid phrasing implying prediction/reproduction of α in the RC body; use "consistent with α_ref" only if strictly needed.
- α-out (experimental, appendix only). If executed, report $\hat{\alpha} \pm \sigma(\hat{\alpha})$ from bootstrap over seeds/resolutions, without using Coulomb-based observables in the estimation pipeline. Pre-register the analysis. PASS/FAIL: $|\hat{\alpha} - \alpha_{ref}| / \alpha_{ref} \leq 1\%$.
- Provenance. Publish seeds, mesh levels, and per-mesh $\hat{\alpha}$ values (continuous-limit trend).
- Scope. This policy governs all RC text, tables, and figures. α is (C) except in the α-out appendix.